An Overview of Solar Radio Type II Bursts through analysis of associated solar and near Earth space weather features during Ascending phase of SC 25

Theogene Ndacyayisenga[1,2], Jean Uwamahoro[3], Jean Claude Uwamahoro[1], Rabiu Babatunde[2], Daniel Okoh[2], Kantepalli Sasikumar Raja[4], Christian Kwisanga[1], and Christian Monstein[5]

[1]University of Rwanda - College of Science and Technology, Kigali, P.O.BOX 3900, Rwanda
[2]Center for Atmospheric Research, National Space Research and Development Agency, Anyigba, Nigeria
[3]University of Rwanda, College of Education, P.O. BOX 55, Rwamagana – Rwanda
[4]Indian Institute of Astrophysics, II Block, Koramangala, Bengaluru - 560 034, India
[5]IRSOL, Istituto Ricerche Solari "Aldo e Cele Daccò", Università della Svizzera italiana, Locarno, Switzerland.

Correspondence: Theogene Ndacyayisenga (ndacyatheogene@gmail.com)

Abstract. Type II solar radio bursts are the signatures of particle acceleration caused by shock waves in the solar atmosphere and interplanetary space. Being electromagnetic radiation that travel at the speed of light, type II radio can serve as proxy to provide early warnings of incoming solar storm disturbances such as geomagnetic storms and radiation storms, which may lead to ionospheric effects. A first observational overview of 31 Type II bursts which occurred in the period between May 2021 to December 2022 is made in solar cycle 25. We analyzed associated parameters such as bandwidth, drift rates, starting frequency to evaluate their dynamical parameters such as the shock and Alfvén speeds to estimate the Alfvén Mach number as well as the coronal magnetic field strength using Rankine-Hugoniot relation. We also evaluated accompanying space weather implication in terms of ionospheric total electron content (TEC) enhancement. At heliocentric distance $\sim 1 - 2\ R\odot$, the shock and the Alfvén speeds are in the range 504 - 1282 kms^{-1} and 368 - 826 kms^{-1}, respectively. The Alfvén Mach number is of the order of $1.2 \leq \mathrm{M_A} \leq 1.8$ at the same heliocentric distance, and the magnetic field strength shows excellent consistency and could be fit with a single power-law distribution of the type $B(r) = 6.1r^{-3.89}\ G$. The current study finds that 18/31 type II radio events are precursors for space weather because they are associated with immediate space weather events such as radio blackouts and polar cap absorption events and exhibit band-splitting features or are followed by type III and IV bursts. Observed and analyzed Type II events correlated well with observed ionospheric storm indicated by the TEC enhancement. The findings from this study indicate that through analysis of type II SRBs observed from the ground and their physical features characteristics, it is possible to monitor the current progress of solar cycle 25 and predict the intensity of associated space weather phenomena.

1 Introduction

The interaction of coronal mass ejections (CMEs) and their shocks with the magnetosphere is the major cause of strongest space weather effects. The energy release from explosive flares also causes perturbations in the Earth's atmosphere (Salmane et al., 2018; Vourlidas et al., 2020). The radio emissions that occur in the solar atmosphere to interplanetary space arise from a

broad range of physical phenomena with space weather implications (e.g., flares, solar energetic particles, CMEs and shocks, Fleishman et al., 2020; Nindos, 2020; Vourlidas et al., 2020). Solar radio bursts (SRBs) originate from different altitudes in the solar atmosphere and they are observed over a wide range of wavelengths from millimeters to centimeters up to meters and decameters. Wild et al. (1963) classified SRBs into five types according to their morphologies of their dynamic spectra and their origin. Of the five types, type II, III and IV bursts are relevant to space weather study because they are associated with space weather drivers, such as shock waves (type II bursts, Cairns et al., 2003; Cane and Erickson, 2005; Chernov and Fomichev, 2021), streams of electrons propagating along open magnetic field lines (type III bursts, Reid and Ratcliffe, 2014, for a review) and CMEs or post-flare loops (type IV bursts, Nindos et al., 2008; Kumari et al., 2021). In the present paper, metric type II radio bursts observed from the ground by extended Compound Astronomical Low frequency Low cost Instrument for Spectroscopy and Transportable Observatory, herein, e-CALLISTO (Benz et al., 2005, 2009) are studied.

First discovered by Payne-Scott et al. (1947), type II radio bursts are among the most powerful events in the solar radio emission observed at metric wavelength (e.g., Wild and McCready, 1950). At present, it is generally accepted that type II radio emissions are excited by magnetohydrodynamic (MHD) shock waves driven by solar flares, CMEs and fast plasma flow in the magnetic reconnection regions (e.g., Maia et al., 2000; Pick et al., 2006; Temmer et al., 2010; Grechnev et al., 2011; Vasanth et al., 2011; Kumari et al., 2017; Gopalswamy et al., 2018; Zucca et al., 2018; Chernov and Fomichev, 2021). Physical properties of metric type II radio bursts including but not limited to drift rate, starting frequency and duration are used to study the dynamics of the middle and upper solar corona. For example, the Alfvén Mach number, $M_A = V_S/V_A$, (V_S and V_A, are shock and Alfvén speeds, respectively) is calculated in three different methods: (i) from shock geometry in EUV images, (ii) by the ratio of the CME speed to the Alfvén speed and (iii) using shock parameters derived from type II radio band-splitting phenomena (Vršnak et al., 2002). A recent study by Maguire et al. (2020) showed that these three methods give consistent results after their comparative analysis.

By analyzing one or two events, many authors (e.g., Cho et al., 2013; Cunha-Silva et al., 2015; Kumari et al., 2017; Maguire et al., 2020; Lata Soni et al., 2021; Kouloumvakos et al., 2021; Mann et al., 2022) have determined the magnetic field strengths and examined the spatial and temporal evolution of shock properties, as well as the conditions responsible for type II radio emissions during high solar activity of solar cycle 24. There have been few works completed during the rise and fall phases of solar cycle 24 (e.g., Gopalswamy and Yashiro, 2011; Vasanth et al., 2014). Kim et al. (2012), on the other hand, covered the entire solar cycle 23. In the current study, a number of events are analyzed during the ascending phase of solar cycle 25 which started in December 2019 (Kallunki et al., 2021; Ahluwalia, 2022; Brajša et al., 2022). We apply the Rankine-Hugoniot density jump relation and parameters of type II radio bursts to estimate the parameter of shock waves (shock and the Alfvén speed, the Alfvén Mach number) of metric type II radio bursts observed by e-CALLISTO and then analyze their space weather implication in terms of the ionospheric total electron content (TEC) enhancement.

2 Observation

2.1 Type II Radio bursts observation

The radio data presented in the current work were observed by e-CALLISTO from May 2021 to December 2022 of solar cycle 25. We started with the list of radio events observed by this instrument hosted at the website (https://e-callisto.org) and selected 31 well separated type II radio bursts whose morphologies are clear, then examined their association with the current solar phenomena to give insights on the status of the ascending phase of the solar cycle 25. In order to investigate the implications of space weather in terms of TEC, each selected type II radio burst was associated with a coronal mass ejection (CME) and the onset of a solar flare. The CME parameters were taken from the Large Angle and Spectrometric COronagraph (LASCO C2) on board the Solar and Heliospheric Observatory (SOHO, Brueckner et al., 1995) catalog updated to 30 December 2022.

2.2 Derivation of shock characteristic parameters

We start this analysis by measuring the bandwidth (BDW) of each type II radio burst. Because all of the type II bursts analyzed lacked the band-splitting feature, the BDW of the fundamental band is linked to the ambient density jump to ensure consistency in computation.

$$BDW = \frac{f_u - f_l}{f_l} \tag{1}$$

where f_u and f_l denote the upper and lower frequencies, respectively of the fundamental emission band. Figure 1 shows an example of type II radio burst from 03:28:25 UT to 03:32:30 UT on April 17, 2022 for which f_u and f_l are indicated. This burst is associated with an X1.1 flare that started at 03:17 UT and stopped at 03:51 UT from NOAA active region 12994. The values of BDW were used to estimate the density jump across the shock (e.g., Vršnak et al., 2001, 2002; Cho et al., 2007; Nedal et al., 2019), χ via the relation

$$\chi = (BDW + 1)^2 \tag{2}$$

By assuming low plasma ratio ($\beta \to 0$) for a perpendicular shock in the corona (Vršnak et al., 2001, 2002), the density jump allows one to compute the Alfvén Mach number (M_A) using Rankine-Hugoniot approximation

$$M_A = \sqrt{\frac{\chi(\chi + 5)}{2(4 - \chi)}} \tag{3}$$

It has been shown that the rate of change of the frequency of metric type II radio bursts is related to the shock speed and the electron density gradient in the solar corona (e.g., Gopalswamy, 2011; Vemareddy et al., 2022) through the relation

$$V_s = -\frac{2r}{\alpha} \left(\frac{1}{f}\right) \left(\frac{df}{dt}\right) \tag{4}$$

where r is the shock formation height, α is a fitted empirical index of density variation over the heliocentric distance, f is the starting frequency, and $\frac{df}{dt}$ is the frequency drift rate. The electron density decreases with heliocentric distance from the
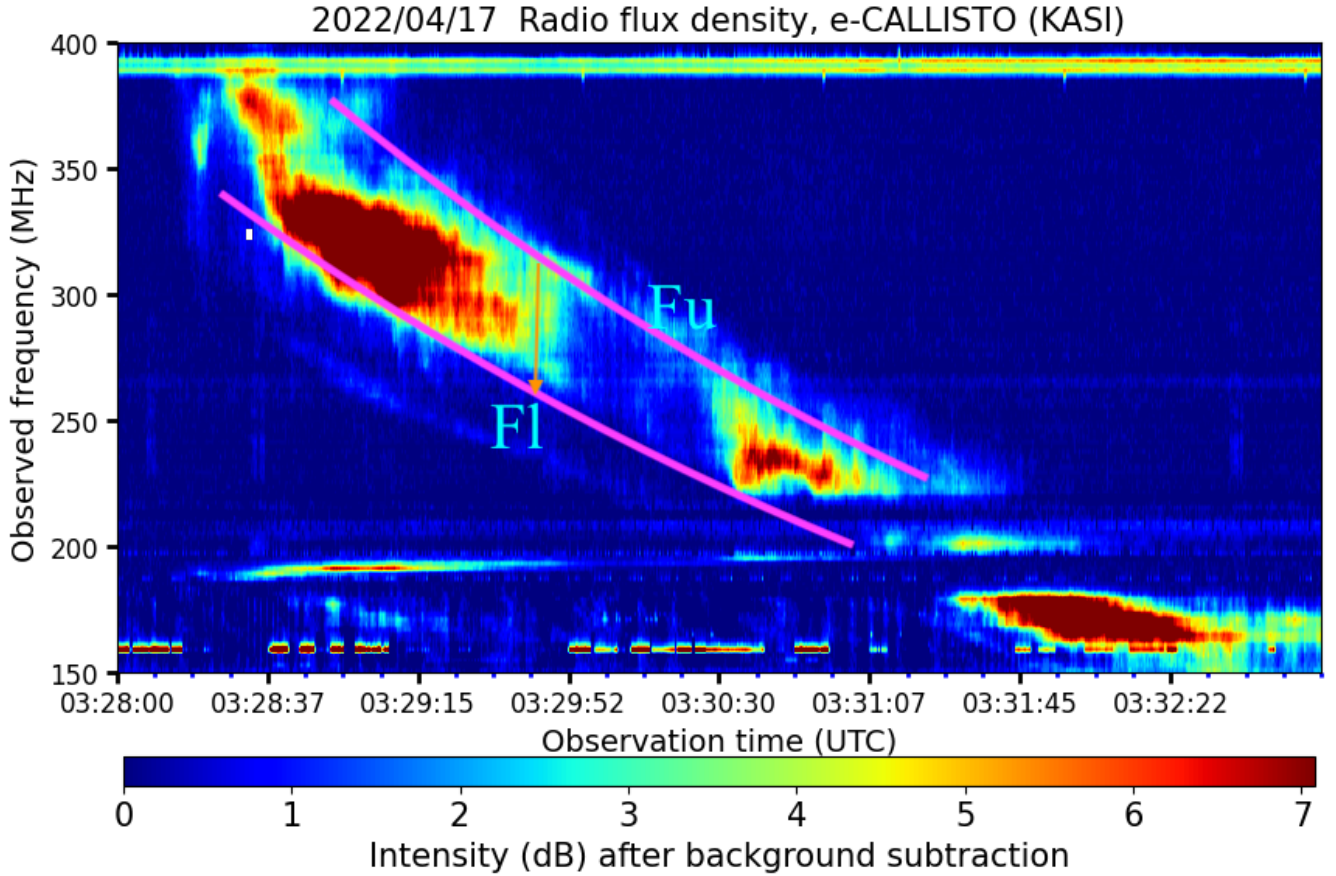
Figure 1. Type II radio burst from 03:28:25 UT to 03:32:30 UT observed by Korean Astronomy and Space science Institute (KASI) on April 17, 2022. F_u and F_l denote the upper and lower frequencies of the fundamental band of the type II radio emission.

Sun, according to the power-law: $n_e(r) \propto r^{-\alpha}$. Three different density models given by Newkirk (1967), Saito et al. (1977) and Leblanc et al. (1998) described the variation of the electron density in the corona and interplanetary medium. With these models, it has been observed that within $1-3$ solar radii $(R_\odot)$, the electron density is directly proportional to r^{-6} in the corona and directly proportional to r^{-2} beyond few tens of solar radii. Because the type II radio observed all have occurred in the range of $\sim 1-2\,R_\odot$, α is chosen to be 6.13 (Gopalswamy, 2011). The Alfvén velocity is directly related to the shock speed as

$$V_A = \frac{V_s}{M_A} \tag{5}$$

In the region surrounding a CME, the ambient magnetic field strength (B) of the plasma can be estimated using the relation (Vršnak et al., 2002; Cho et al., 2007; Lata Soni et al., 2021)

$$B[G] = 5.1 \times 10^{-5} \times f_l[MHz] \times V_A[km/s] \tag{6}$$

 ## 2.3 Ionospheric Data

GPS data from ground-based GPS receiver stations around the world were used to analyze the ionospheric total electron content (TEC) for disturbed days identified by type II radio burst observations in this study. These include the African Geodetic Reference Frame (AFREF) database (http://afrefdata.org/) and UNAVCO Archive of GNSS Data (https://www.unavco.org/). As GPS data are usually provided in Receiver Independent EXchange (RINEX) format, TEC were derived from Rinex files using the GPS TEC software developed at Boston college, assuming a thin shell ionosphere at the altitude of 350 km. Details on the software used to derive TEC are provided in Seemala and Valladares (2011); Uwamahoro et al. (2018, and references therein).

3 Results and Discussions

3.1 Comparison and analysis

During the ascending phase of the solar cycle 25, the e-CALLISTO network observed a series of solar radio bursts in the range from 10 MHz to 870 MHz. With the interest of space weather diagnostics, 31 well separated type II radio bursts observed by this network are presented in this study. Table 1 lists the CALLISTO Spectrometers used in this study, as well as their geographic locations, frequency range of observation, and number of radio bursts taken at each station. According to this table, all radio spectrometers are observing in a narrow frequency range. Using the radio parameters such as bandwidth, drift rate and

Table 1. e-CALLISTO Spectrometers, their geographical locations and their frequency ranges.

#	File ID	Country	Lat(deg)	Long (deg)	Obs. Frequency range (MHz)	# of events
1	Australia$_-$ASSA	South Australia	-30.00	136.21	15 — 87	11
2	Arecibo$_O$bservatory	Puerto Rico, USA	18.22	-66.59	15 — 87	9
3	GREENLAND	Greenland	67.00	-50.72	10 — 110	3
4	ALASKA$_-$HAARP	ALASKA	64.84	-147.72	5 — 87	2
5	ALMATY	Kazakhstan	43.22	76.83	45 — 165	1
6	BIR	Ireland	16.61	77.51	10 — 100	1
7	INDIAN$_-$OOTY	India	11.41	76.69	45 — 165	1
8	KASI	South Korea	36.35	127.38	150 — 400	1
9	MEXICO$_L$ANCE	MEXICO	19.81	-101.69	50 — 90	1
10	SWISS-Landschlacht	Switzerland	47.63	9.25	15 — 87	1

starting frequency, the shock characteristics from each radio event have been estimated. Table 2 illustrates each type II radio burst selected and associated CME , GOES soft X-ray flares as well as shock characteristics. The first column of this table is the numbering index of the events, the next four columns are the date of the radio events in the format dd/mm/yyyy hh:mm, their starting frequencies, f (MHz), their drift rates (MHz/s) and their shock formation heights ($R_\odot$) estimated using the rela-

tion $f(r) = 307.87r^{-3.78} - 0.14$ (Gopalswamy et al., 2013). Columns 6 to 9 are the GOES soft X-ray flares parameters (start, class, NOAA region and location) followed by two columns that present the CME onset and speed, respectively. Columns 12 to 15 present the shock characteristics (density jumps, Mach numbers, shock and Alfvén velocities, respectively) while the last column of this table presents the estimated ambient magnetic field strength, B (Gauss). There is a strong correlation (CC=0.97)

Table 2. Type II radio bursts observed by e-CALLISTO during the ascending phase of solar cycle 25 and their associated CMEs, GOES soft-Xray flares and estimated shock characteristics.

No	Type II burst event				Soft X-ray flare				CME		Shock characteristics				B-field
	Date	f	Drift rate	height	Start	Class	NOAA	Location	Onset	Speed	χ	M	V_s	V_A	
	(UT)	(MHz)	(MHzs^{-1})	$R_\odot$	(UT)				(UT)	(kms^{-1})			(kms^{-1})	(kms^{-1})	G
1	22/05/2021 02:57	86	- 0.13	1.4	02:47	C6.1	12824	N18E25	......	.....	1.6	1.5	752	504	1.5
2	23/06/2021 07:05	73	-0.10	1.5	06:43	C3.4	12833	N14E89	07:24	390	1.5	1.4	668	464	1.2
3	25/07/2021 04:54	64	-0.11	1.5	.....	....	F. S.	......	05:48	237	1.3	1.2	785	637	1.6
4	28/08/2021 05:10	64	-0.11	1.5	05:01	C7.0	12860	S31E06	.....	.....	1.7	1.6	894	556	1.2
5	09/10/2021 06:34	75	- 0.12	1.5	06:19	M1.6	12882	N18E06	07:00	712	1.6	1.5	790	533	1.4
6	09/10/2021 06:49	31	- 0.04	1.9	06:19	M1.6	12882	N18E06	07:00	712	1.3	1.3	706	561	0.7
7	20/12/2021 11:27	87	- 0.16	1.4	11:12	M1.8	12908	S20W01	12:36	386	1.7	1.6	860	549	1.7
8	12/01/2022 04:28	69	- 0.17	1.5	.....	....	F. S.	......	03:12	433	1.8	1.7	1261	740	1.7
9	12/02/2022 08:33	173	- 0.36	1.2	08:25	M1.4	12939	S17W82	08:12	785	1.3	1.2	792	659	4.1
10	02/03/2022 17:42	67	- 0.11	1.5	17:31	M2.0	12958	N15E29	18:24	248	1.9	1.7	924	532	1.1
11	14/03/2022 17:20	98	- 0.13	1.4	17:13	B8.5	12964	S30W86	17:48	534	1.9	1.7	883	506	1.2
12	25/03/2022 05:15	66	- 0.12	1.5	05:02	M1.4	12974	S18E37	06:12	433	1.5	1.4	801	590	1.6
13	28/03/2022 11:23	87	- 0.15	1.4	10:58	M4.0	12975	N18W04	12:12	335	1.8	1.7	951	554	1.4
14	30/03/2022 17:33	72	- 0.11	1.5	17:21	X1.3	12975	N13W31	18:00	493	1.9	1.8	1128	654	1.1
15	31/03/2022 18:34	67	- 0.13	1.5	18:17	M9.6	12975	N12W47	18:53	639	2.0	1.8	1081	594	1.3
16	02/04/2022 13:24	71	- 0.15	1.5	12:56.	M3.9	12975	N12W68	13:36	686	1.8	1.6	1038	631	1.5
17	17/04/2022 03:28	382	- 0.83	0.9	03:17	X1.1	12994	N12E88	03:48	728	1.2	1.2	828	711	7.8
18	21/04/2022 02:00	85	-0.15	1.4	01:47	M9.6	12993	N22E23	02:36	828	1.7	1.5	1070	696	1.6
19	21/04/2022 22:47	69	-0.11	1.5	22:39	C1.6	12993	N12E25	23:12	389	1.4	1.3	791	591	1.4
20	30/04/2022 13:46	83	-0.13	1.4	13:37	X1.1	12994	N16W88	14:00	535	1.7	1.5	936	610	1.4
21	30/04/2022 19:50	80	-0.12	1.4	19:42	M1.9	12994	N16W88	20:12	793	1.7	1.6	855	543	1.3
22	04/07/2022 13:35	69	-0.13	1.5	12:23	C5.1	13050	N17E36	11:36	256	1.7	1.6	918	581	1.4
23	05/07/2022 04:16	69	-0.10	1.5	03:59	C9.8	13045	S20W18	05:00	515	1.6	1.5	761	512	1.2
24	14/08/2022 12:05	70	-0.08	1.5	11:50	C2.4	13076	N21W14	13:25	411	1.4	1.3	512	402	1.1
25	18/08/2022 12:12	62	-0.16	1.6	.....	....	F. S.	......	11:00	1131	1.7	1.6	1282	826	1.9
26	19/08/2022 04:35	81	-0.10	1.4	04:14	M1.6	13078	S27W48	04:49	695	1.3	1.2	504	420	1.4
27	23/09/2022 18:02	67	-0.13	1.5	17:48	M1.7	13110	N16E84	18:12	687	2.0	1.8	1095	594	1.2
28	29/09/2022 12:06	80	-0.10	1.4	11:50	C5.7	.....	N26E86	12:24	321	1.5	1.4	672	473	1.2
29	09/11/2022 20:03	89	-0.11	1.4	.....	....	F. S.	......	20:36	371	1.5	1.4	618	435	1.3
30	03/12/2022 17:44	84	-0.13	1.4	17:36	M1.2	13157	N14E89	.....	.....	1.8	1.8	857	518	1.3
31	14/12/2022 08:30	160	-0.22	1.2	08:24	M1.1	13162	S16W89	08:48	402	1.9	1.8	657	368	1.7

between the drift rates and starting frequencies of the type II radio bursts (Figure 2) which are the key parameters to estimate the shock speeds from the dynamic spectra. Higher starting frequency have higher drift rates (Umuhire et al., 2021). Such correlation agrees well with the previous studies, giving slopes of $\epsilon = 1.89$ and $\epsilon = 1.33$, respectively (e.g., Vršnak et al., 2002; Umuhire et al., 2021). From Table 2, it is clearly observed that 4/31 radio events are not associated with any solar flare because
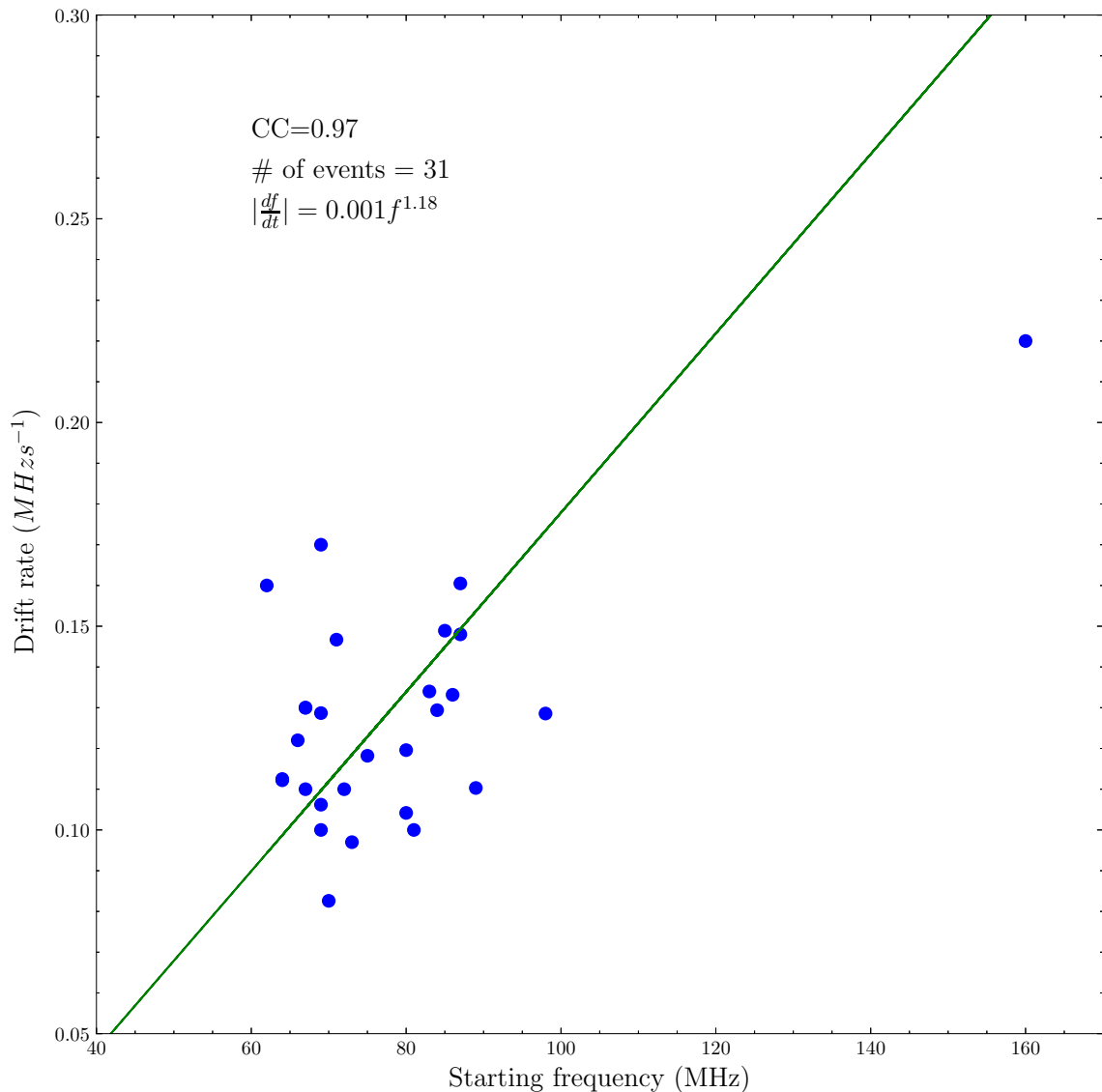
Figure 2. Scatter plot between the absolute drift rates ($|\frac{df}{dt}|$) and the starting frequency (f_s) for all the 31 metric type II radio bursts. The power-law least squares fits and the corresponding correlation coefficient Cc are shown.

they originate from farside on the solar surface but the shocks generating these bursts were excited by associated CMEs. It is also noticed that 18/27 are connected with intense GOES X-ray flares (M & X classes), which is compatible with their speeds as well as estimated shock speeds. We derived the shock and Alfvén speeds of these type II radio bursts in the order of 504 - 1282 $\mathrm{kms^{-1}}$ and 368 - 826 $\mathrm{kms^{-1}}$, respectively at heliocentric distance $\sim 1 - 2\ R_\odot$. Comparatively, values are consistent with the measurements reported by Cunha-Silva et al. (2015); Minta et al. (2023) about 590 - 810 $\mathrm{kms^{-1}}$ and 250 - 550 $\mathrm{kms^{-1}}$,

respectively at $\sim 1.2 - 1.8\ R_\odot$. The Alfvén speeds from the current work are also in agreement with the range of the Alfvén speeds of $140 - 460\ \mathrm{kms}^{-1}$ over $1.2 - 1.5\ \mathrm{R}_\odot$ and $259 - 982\ \mathrm{kms}^{-1}$ over 3 - 15 $\mathrm{R}_\odot$ given in Gopalswamy et al. (2011a) and in Kim et al. (2012), respectively. Figure 3 presents the correlation between the speeds from the LASCO field of view (FOV) and the speeds derived from the dynamic spectra. Table 2 observations and Figure 3 show that there are estimated shock speeds
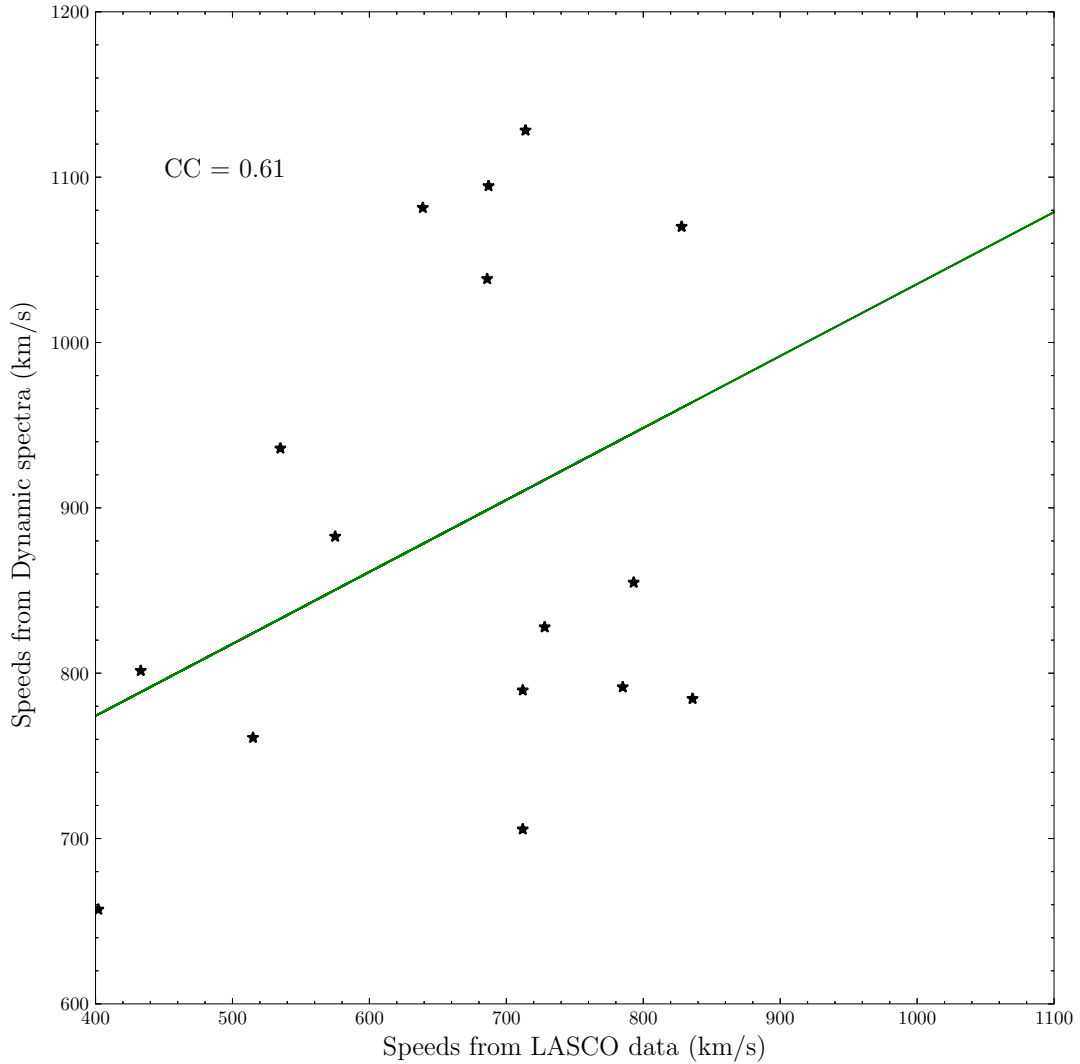
Figure 3. Scatter plots showing the correlation between the speeds from LASCO FOV and speeds derived from dynamic spectra. Higher values of speeds obtained from dynamic spectra are attributed to the radio source, which propagates at faster speeds due to the interaction of slow CMEs with background magnetized coronal plasma (Tan et al., 2019).

125

that are faster than CME speeds from LASCO FOV and vice versa. The difference in CME speed between dynamic spectra and LASCO is attributed to the CME's central position angle as observed by LASCO, implying that the shock may be weakened

and dissipated before entering LASCO FOV (Gopalswamy et al., 2011b). On the other hand, the shock decelerates in the case of a decline in its intensity or when it breaks. The type II burst only serves as a time marker for when the shock occurs. It should be noted that type II radio emission can come from anywhere on the shock front: the nose or the flanks, depending on which location is best for electron acceleration (Gopalswamy et al., 2013). Solar radio type II bursts associated with slow CMEs are thought to be generated from non-thermal electrons accelerated by a moving magnetic reconnection when slow CMEs interact with the background magnetized coronal plasma (Tan et al., 2019). Furthermore, a recent study confirmed that observing a type II radio burst is evidence of shock acceleration in the solar corona (Chernov and Fomichev, 2021).

The Alfvén Mach numbers in the range $\sim 1.2-1.8$ at $\sim 1-2\,\mathrm{R}_\odot$ are consistent with the measurements of about 1.1 - 1.9 at $\sim 1.3-2.5\,\mathrm{R}\odot$ reported by Vršnak et al. (2002) and that of Cunha-Silva et al. (2015) in the order of 1.4 to 1.7 at $\sim 1.2-1.8\,\mathrm{R}_\odot$. The magnetic field strength is an important parameter that influences the dynamical eruption of CMEs in the solar atmosphere (e.g., Sasikumar Raja et al., 2014; Carley et al., 2017). High-starting type II radio bursts are associated with coronal shocks that are closer to the solar surface. As a result, high magnetic field values are expected. Figure 4 demonstrates the variation of the magnetic field strength estimated in this study (Equation 6) relative to the quiet Sun magnetic field model $B(r) = \frac{a}{r^2}$ with $a = 2.2$ (Gopalswamy et al., 2001) and Dulk and McLean (1978) empirical model for the magnetic field above active region $B(r) = 0.5\,(r-1)^{-1.5}$. The magnetic field has been calculated in the range $0.6 < B < 8\,G$ at $\sim 1-2\,\mathrm{R}_\odot$, which shows excellent consistency with earlier researches and is fitted with a single power-law distribution of the type $B(r) = 6.1r^{-3.89}\,G$ as represented by the black dotted curved of Figure 4. However, Rankine - Hugoniot jump relation has been used by a number of researchers to derive shock parameters. For example, with this technique Smerd et al. (1974, 1975) found $1.2 \leq \mathrm{M_A} \leq 1.7$ and $0.3 \leq \mathrm{B} \leq 4$ G. The same technique was applied by Vršnak et al. (2002) who reported a magnetic field strength in the range 1 - 8 G at heliocentric distance of $\sim 1.6\,R_\odot$. A field strength of 6 - 5 G at $\sim 1.5-1.77\,\mathrm{R}_\odot$ is reported by Ramesh et al. (2010). Dulk and McLean (1978); Sasikumar Raja et al. (2022) have given a detailed review on solar coronal magnetic fields measured using different techniques and at different wavelengths of the electromagnetic spectrum. A recent work has reported that two necessary conditions for type II radio emissions are: (i) relatively intense shock waves (the Mach number should exceed a certain value $\mathrm{M_{cr}}$) and (ii) perpendicular shock waves are required (Chernov and Fomichev, 2021). Our values of Mach numbers $1.2 \leq \mathrm{M_A} \leq 1.8$ agrees well with these conditions. In Table 3, the statistical findings from this study and earlier research that examined more than two radio events are summarized and compared.

Table 3. Comparison of the statistical findings of this study and previous studies that analyzed more than two radio events.

Epoch	# of events	Mean shock speed (km/s)	Mean Alfvén speed	B-field range (G)	Height range $(R_\odot)$	# Authors
2021 − 2022	31	860	566	8 − 0.6	1.0 — 2.0	This work
2013 − 2014	4	739	579	1.8 − 1.3	1.7 − 1.9	Kishore et al. (2016)
1996 − 2007	10	1288	555	0.105 − 0.006	3 − 15.	Kim et al. (2012)
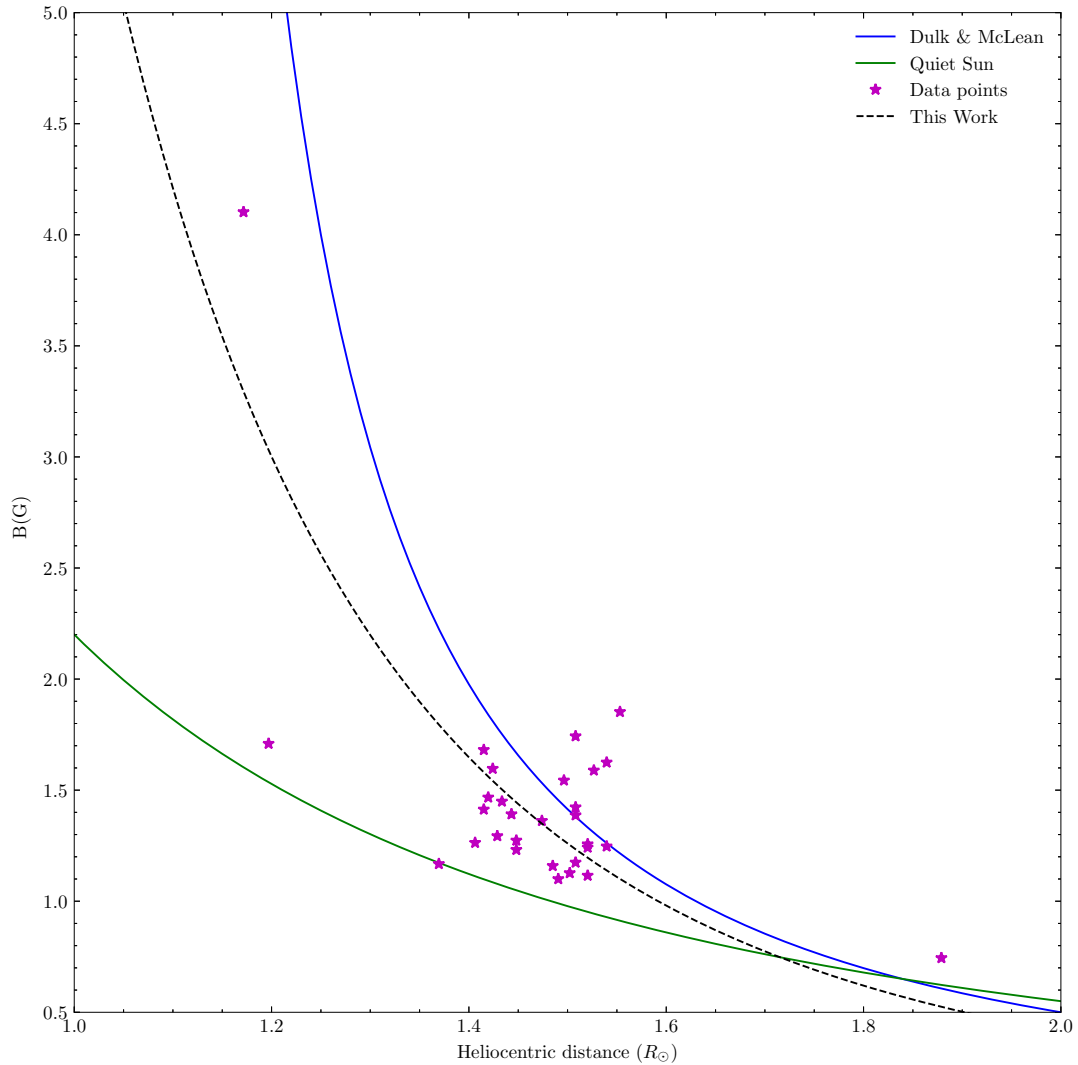
Figure 4. Comparison of the magnetic field strength from the current study, the quiet Sun magnetic field model (Gopalswamy et al., 2001) and the empirical magnetic field relation (Dulk and McLean, 1978). The magnetic values estimated are all above the quiet Sun magnetic model and the pattern is close to the empirical mode which confirms that the Sun was awake.

3.2 Associated Space weather implication

The ascending phase of solar cycle 25 is characterized by high solar activity than expected (SW, 2022). This is indicated by a number of space weather events that have been registered by SWPC. Tan (2011) and Sarp et al. (2018) show that solar cycle 25 is more active than the previous cycle and is more consistent with actual observations as predicted. Furthermore, Du (2020) estimated that the maximum peak of cycle 25 would be 30% stronger than that of cycle 24. These indicate that the activity

would be high, and we use this advantage to track the intensity of early space weather events in the current cycle. Because of their connection to solar phenomena (e.g., radio blackouts), Type II solar radio bursts were used as selection criteria for disturbed days. The TEC was examined on 24 type II radio bursts, which are linked to both solar flares and CMEs, by selecting GNSS stations in either equatorial, mid-latitude, and high-latitude regions. The TEC enhancements of 8 – 11 October 2021 (DOY=281 – 284) and 24 March – 3 April 2022 (DOY=83 – 93), in particular, are used as illustrative examples, along with their corresponding type II radio events, to highlight some space weather hazards observed.

3.2.1 October 9, 2021 event

Type II radio bursts on 2021 October 9, was recorded among other spectrometers of e-CALLISTO by Astronomical Society of South Australia (Australia-ASSA): the first type II burst is recorded in the time range of 06:34 UT to 06:42 UT overlapped by a type IV radio burst from 06:37 UT to 06:46 UT. Another type II radio burst is registered from 06:49 UT to 06:55 UT with band-splitting feature as it is displayed in the top panel of Figure 5. All of these events are associated by GOES soft X-ray flare of M1.6 class that started at 06:19 UT, peaked at 06:38 UT and stopped at 06:53 UT from NOAA Active region (AR) 12882 explosion. They are also associated with a halo CME observed by LASCO C2 coronagraph with onset at 07:00 UT with a speed of $712 \, \mathrm{kms}^{-1}$. This CME has reached near Earth on 2021 October 12 and caused a geomagnetic storm at 14:30 UT with Dst = -65 nT. It is observed that few minutes after the first type II has started, an enhancement of protons took place as an effect of radio blackout depicted in bottom of Figure 5. It is noted that the flare has no direct interaction with the magnetosphere but its radiation agents (X-rays, UV, EUV) perturb the ionosphere by increasing the ionization which in turn causes the signal delay in Global Navigation Satellite Systems (GNSS) (e.g., Amory-Mazaudier et al., 2017). Table 4 lists the codes, country, geographic and geomagnetic coordinates of some GNSS stations used in the current study for a reference. Figures 6 (a) and (b)

Table 4. Geographic and Geometric coordinates of some GNSS stations used for this study

| Code | Country | Geographic coordinates | | Geomagnetic Coordinates | | |
		Lat(deg)	Long (deg)	Lat(deg)	Long (deg)	Altitude (m)
abpo	Madagascar	-19.018	47.229	-23.30	116.73	1552.992
bogt	Colombia	4.640	74.081	13.87	-1.46	2576.778
falk	Falkland Island	-51.694	-57.874	-52.50	12.44	50.841
iisc	India	13.021	77.570	4.86	150.94	843.713
mbar	Uganda	-0.601	30.738	-2.73	103.13	1337.653

show the variations in ionospheric total electron content (TEC) after flares and radio bursts from two affected stations, one in Africa and the other from Asia, the regions affected during the radio blackout. The diurnal variations shown in Figure 6 (a) are as follows: At 06:35 UT, the TEC units (TECU, 1 TECU = 10^{16} electrons/m^2) over Madagascar (abpo) are 19 TECU, 18.5 TECU, 17.5 TECU, and 25 TECU, respectively, and at 12:00 UT, the trend is 21 TECU, 25 TECU, 18 TECU, and 19 TECU, respectively, for the period 8 - 11 October 2021 (DOY=281 – 284). TEC variations at Bangalore station (iisc) in Figure 6 (b) at
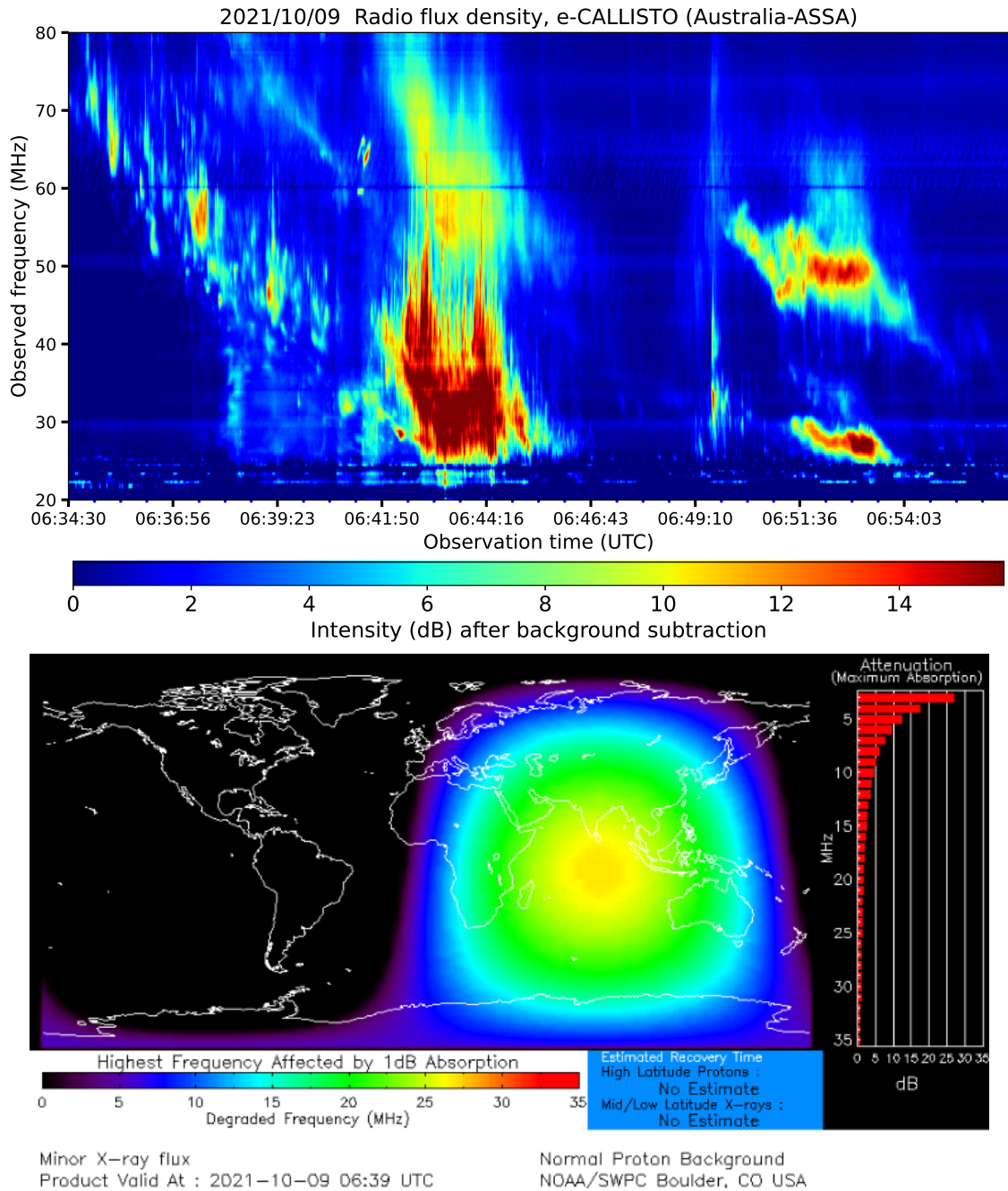
Figure 5. The top panel shows type II radio emissions that are observed on 2021 October 9. Lower panel shows a minor radio blackout that occurred over Africa, the Indian Ocean, Europe , Australia and Asia on 2021 October 9 due to the enhancement of X-ray flux and UV radiation at the Earth. Credited to the SWPC.
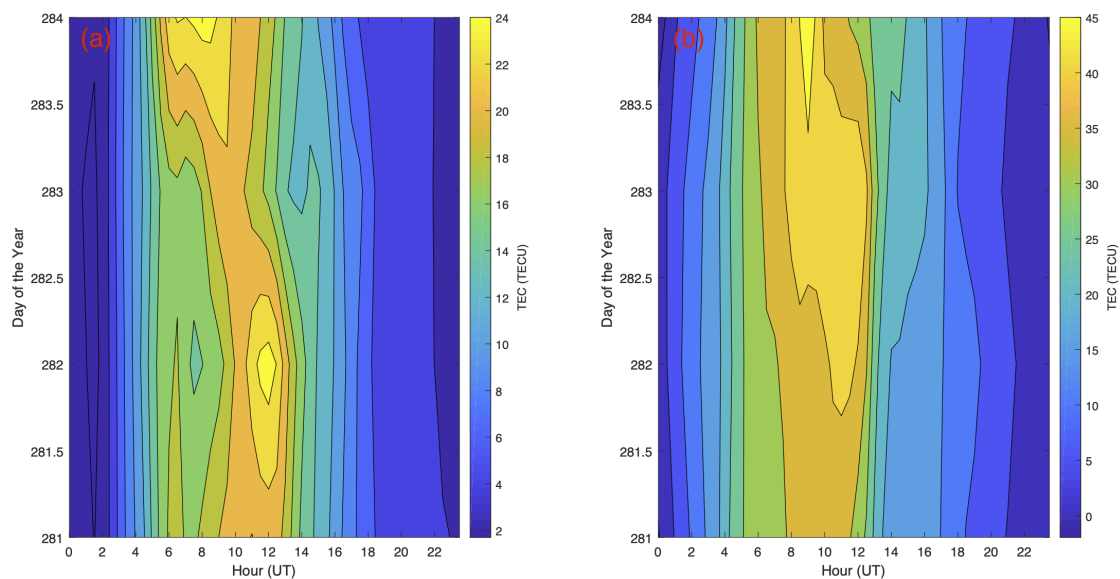
Figure 6. Four-day contour maps of (a) TEC over Madagascar (abpo) and (b) TEC over India (iisc) between 8 – 11 October 2021 (DOY=281 – 284). The maximum TEC over Antananarivo on each day is 21 TECU, 25 TECU, 18 TECU and 19 TECU, respectively at around 12:00 UT. These are 40 TECU, 38 TECU, 44 TECU and 49 TECU at 09:00 UT over Bangalore station.

06:35 UT are 32 TECU, 34 TECU, 35 TECU, and 37 TECU, respectively. At 09:00 UT, the trend was 40 TECU, 38 TECU, 44 TECU, and 49 TECU, respectively. The Kp indices for these four days are 2, 2, 4, and 3, respectively. The variations in TECs between the two stations are significant, and are caused by flares and/or corotating interaction regions (CIRs).

3.2.2   March 24 - April 1, 2022

The solar activity is seen to be high during March 2022. This is due to a number of solar events observed and recorded during this month. In fact, seven type II radio events were recorded in March 2022. Four of the seven events are in close proximity, are associated with CMEs of mean speed of 472 km/s and mean estimated shock speed of 990 km/s. Figure 7 presents a type II radio burst observed by e-CALLISTO network at Arecibo Observatory in Puerto Rico, USA from 11:23:12 UT to 11:28:37 UT on 28 March 2022 with 87 - 32 MHz frequency range. This burst is overlapped by a type IV radio burst that occurred from 11:26 UT to 11:36 UT. These bursts are associated with GOES soft X-ray flare M4.0 that started at 10:58 UT, peaked at 11:29 UT and stopped at 11:45 UT from NOAA 12975. This eruption also produced a tsunami in the solar atmosphere (see, https://sdo.gsfc.nasa.gov/data/dailymov/movie.php?q=20220328_1024_0193). The bursts are also associated with a partial halo CME with speed of 335 kms^{-1} and the CME was off Sun - Earth line because no geomagnetic storm is linked to it. However, the flare and the tsunami accelerated protons that hit the Earth's magnetosphere and caused a minor radiation storm. The enhancement of proton events is revealed by the radio blackout that cover the whole African continent (see
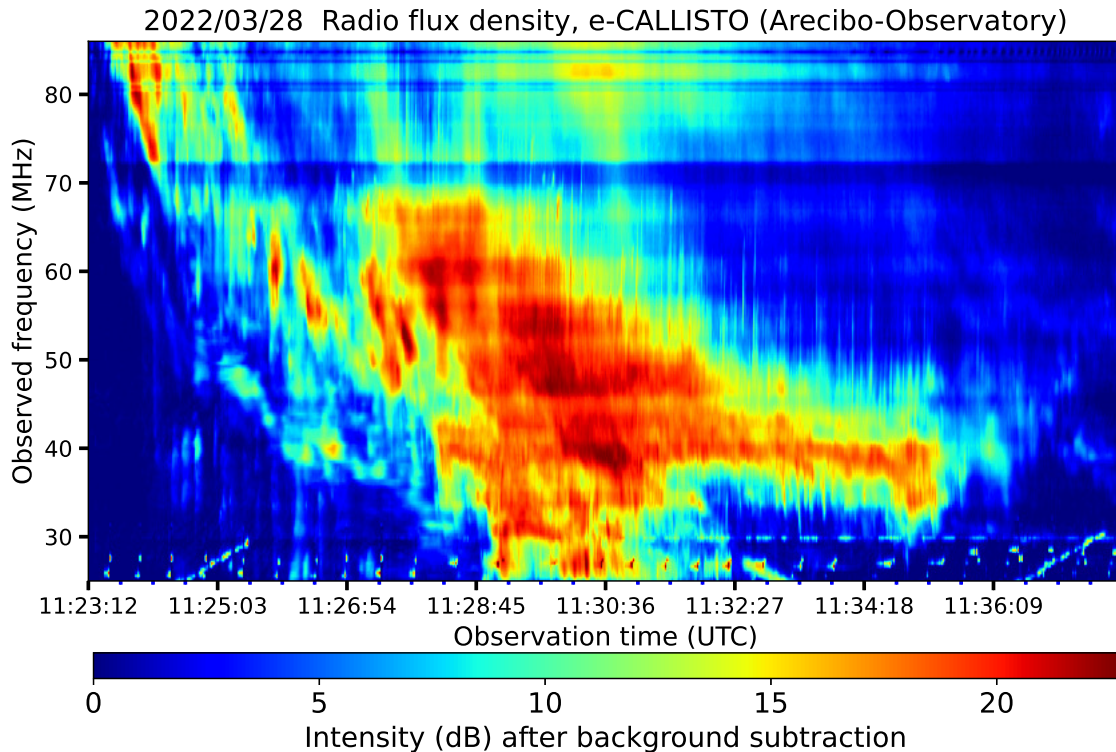
Figure 7. The type II radio emissions that are observed on March 28, 2022 from 11:23:12 UT to 11:28:37 UT followed by a type IV radio bursts from 11:26 UT to 11:36 UT.

top panel of Figure 8). The lower panel of Figure 8 shows the polar cap absorption event (PCAE) that occurred after about 2:40 UT from the burst onset. This event is a signature of solar proton enhancement where high frequency (HF) and very HF (VHF) are absorbed and low and very low frequencies are reflected at low altitude. Previous works showed that solar flares that cause solar proton events (SPEs) are usually accompanied by radio bursts and noise storms that disturb the ionospheric TEC (Ranta et al., 1993); and mostly observed 20 minutes to 20 hours after the solar flare (Mitra, 1974; Kavanagh et al., 2004; Perrone et al., 2004). They also showed that SPEs and PCAEs are frequent close to the maximum solar cycle (Shea and Smart, 2002), but the solar cycle 25 is far from its maximum. Thus, these observations are the evidence of high solar activity during the ascending phase of the current sunspot cycle. It is important to note that the association of type II radio bursts with space weather drivers such as solar flares, SPEs and coronal mass ejections make them special for space weather (Kumari et al., 2019; Ndacyayisenga et al., 2021b). Using contour maps, Figure 9 shows the diurnal variation of TEC over four different stations (mbar: Mbarara, abpo: Madagascar, falk: Falkland Islands and bogt: Bogota) during 24 March – 3 April 2022 (DOY=83 – 93) The geographic and geomagnetic coordinates of these stations are given in Table 4. Because of their geographic and geomagnetic coordinates, the first two stations provide maximum TEC between 11:00 UT and 12:00 UT, while the last two provide maximum TEC between 16:00 UT and 18:00 UT. The GNSS station shown in Figure 9 (a) experienced 5 TECU drop on 26 March 2022
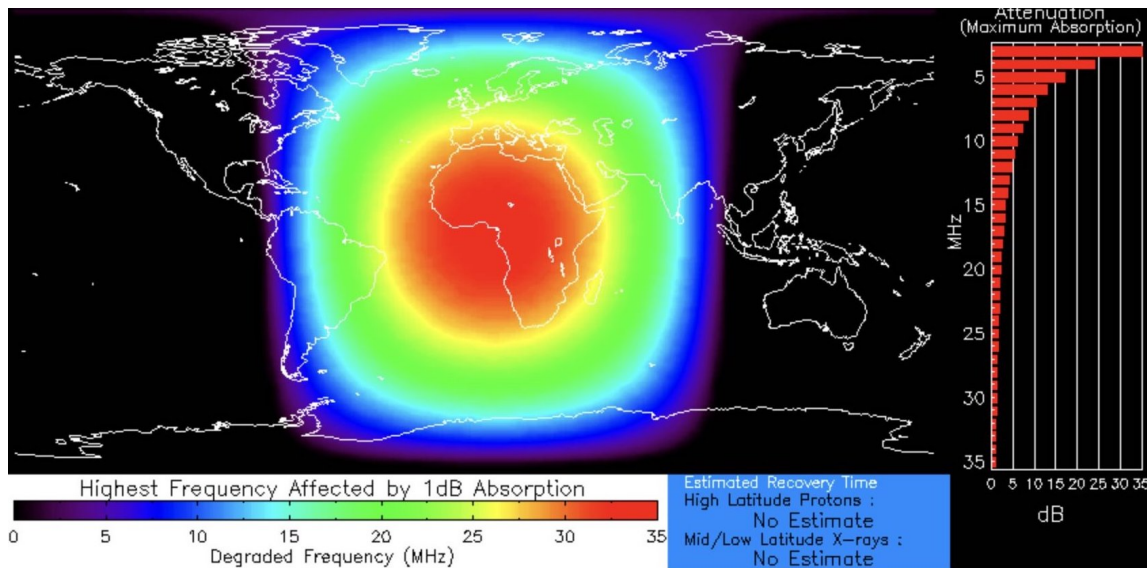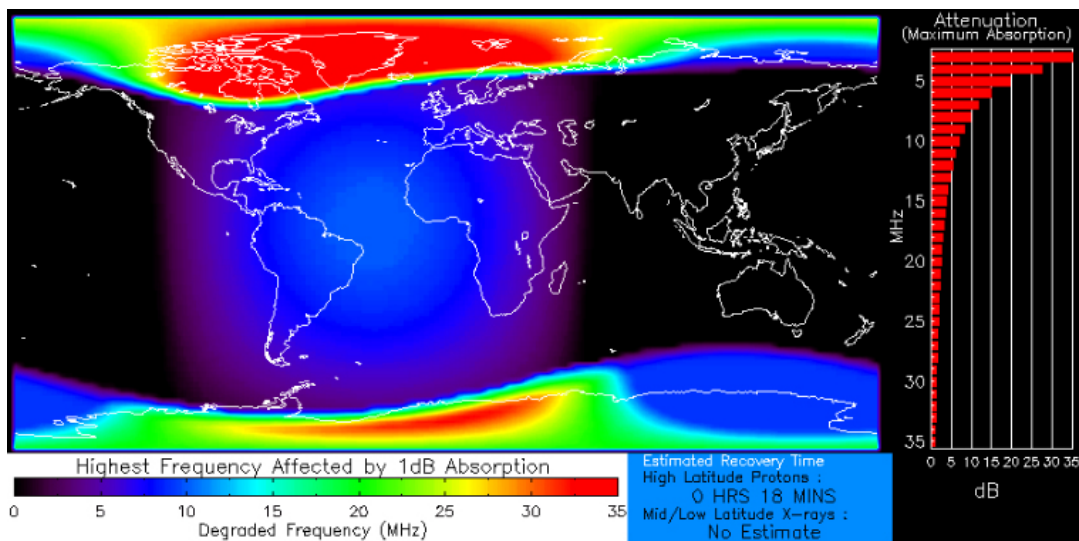
Figure 8. Top panel: The radio blackout due to proton enhancement induced by a M4.0 flare on March 28, 2022. Lower panel shows a polar cap absorption event that occurred 2:40 UT after the registration of type II on March 28, 2022 due to solar energetic particle acceleration. Credited to the SWPC.

(DOY=85) and TEC enhancements of 8 and 12 TECU on 29 March (DOY=88) and 31 March 2022 (DOY=90), respectively. Such drop and enhancements are caused by solar flares and CIR (Kp=5), respectively. It can be seen that between 08:00 UT
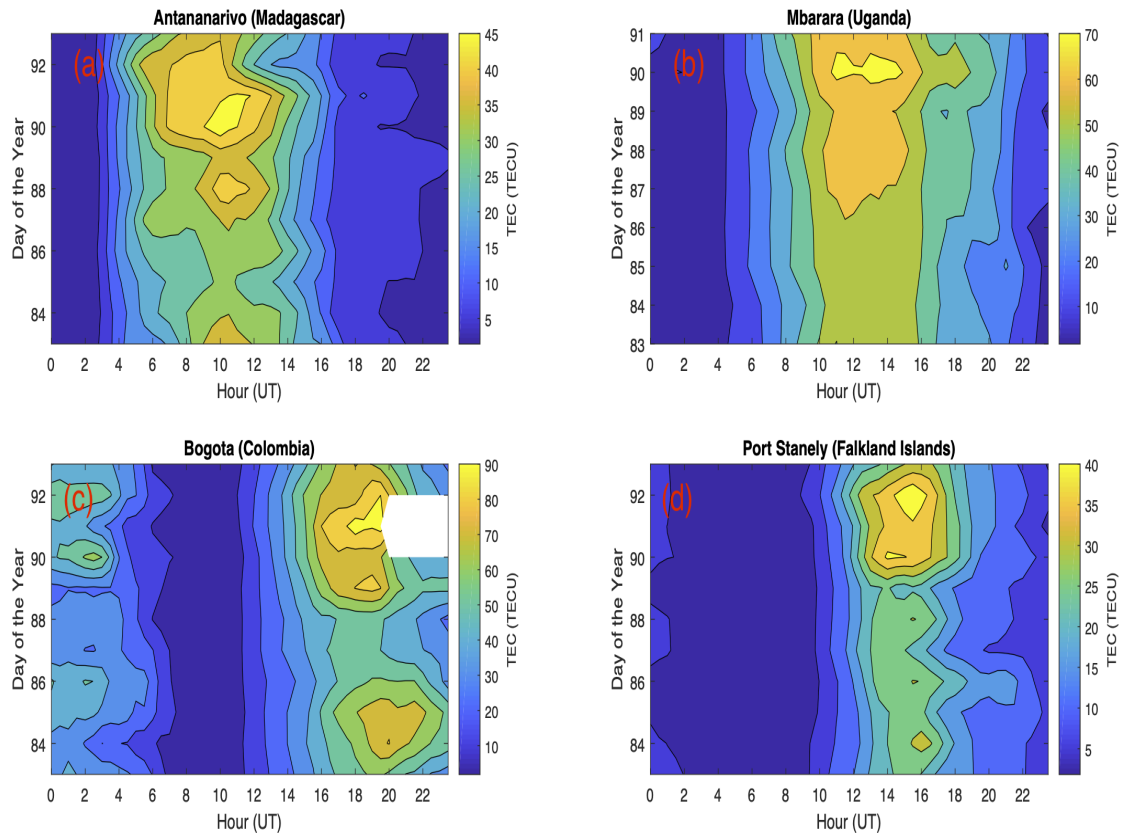
Figure 9. The eleven contour TEC plots of DOY=83 – 93 (24 March – 3 April 2022) (a) 0ver Antananarivo station (Madagascar), (b) over Mbarara station (Uganda), (c) over Bogota station (Colombia) and (d) over Port Stanley station (Falkland Islands, South Atlantic ocean), respectively.

and 16:00 UT on 24 – 26 March 2022 (DOY=83 – 85) the TEC is lower than on subsequent days. These TEC fluctuations are associated with Kp indices of 3, 3, 3, 4, 4, 3, 3, 5, 4, 5 and 4 indicating that the days are nearly perturbed, which is a signature of incoming radiation agents occurring in succession on a daily basis. Figure 9 (b) depicts the trend of TEC variation decreasing by 10 TECU on 26 March 2022 (DOY =85), compared to normal TEC (normal maximum TEC=65 TECU), and an increasing by 8 TECU on 31 March 2022 (DOY=90). The solar flare is responsible for the decrease in TEC on 26 March 2022 (DOY=85), and the CIR with Kp=5 is attributed to the cause of the increase in TEC on 31 March 2022 (DOY=90). However, this station presented in Figure 9 (b) is located in equatorial region. The anomaly is thought to be caused by either (i) the weather condition near the Earth's equator, (ii) the effects of previous perturbations and/or (iii) equatorial ionization anomaly. On the other hand, Figure 9 (c) and (d) present two stations in high latitudes (North and south hemisphere, respectively). At both stations, the TEC is low between 00:00 – 12:00 UT because this time range covers the night time. A prominent TEC enhancement is observed

from 15:00 UT to 21:00 UT at Bogota station (Figure 9 (c)) during 30 March – 1 April 2022 (DOY=89 - 91). The trend of TEC variation at this station is given by the variation of TEC maxima of the order of 56, 59, 68, 56, 52, 52, 78, 76, 92, 73 and 70 TECU, respectively at 18:00 UT, corresponding to the same Kp indices. Figure 9 (d) shows that the diurnal variation of TEC is increased by more than 24 TECU on a daily basis on 25 – 26 (DOY=84 – 85), 30 – 31 March (DOY=89 – 90), and 1 April 2022 (DOY=91), due to CIR (Kp=4), solar flare, and CIR (Kp=5), respectively, over Bogota station. The variations of TEC over these stations are attributed to the ionizing flux from flares and CIR. The diurnal variation is prominent at all stations, which corresponds to daily strong flares, radio blackouts, and polar cap absorption events recorded between 24 March 25 – 3 April 2022 (DOY=83 – 93) as a result of particle enhancement. It is worth noting that agencies that rely on GPS signals located in the areas depicted in Figure 9 (a) – (d) may have experienced signal delays or loss as a result of ionospheric disturbances that occurred between 24 March and 1 April 2022. Smith et al. (2017) investigated global auroral ovals using magnetic data from near-Earth orbit satellites. Their investigation is limited to auroral electrojet currents for $Kp \leq 4$, and they propose (in figure 7) that increasing Kp by 2 results in a roughly doubling of auroral electrojet current strength for $0 \leq K_p \leq 4$. It is clear from the examples above that type II radio bursts can be used as a warning of impending space weather hazards. Because they are either connected to immediate space weather events like radio blackouts or polar cap absorption events, exhibit band-splitting properties, or are followed by type III or IV radio bursts, 18 of the 24 type II radio events in the current study are potentially space weather precursors. The other 7 radio bursts display normal space weather. Solar radio bursts are among the first signs of erupting events in the solar corona to be observed (Salmane et al., 2018; Ndacyayisenga et al., 2021a).

4   Summary and conclusion

In this study, we report on an analysis of 31 well separated type II radio bursts observed by e-CALLISTO network from May 2021 to December 2022. The parameters of type II radio bursts, such as bandwidth, drift rates and starting frequency are used to derive the corresponding shock parameters: the shock speed, Alfvén speed, Mach number and magnetic field strength. The shock and Alfvén speeds are estimated in the range of 504 - 1282 kms^{-1} and 368 - 826 kms^{-1}, respectively at heliocentric distance $\sim 1 - 2\,\mathrm{R}_\odot$. The range of measurements that is consistent with the earlier works including the Alfvén speed with 550 - 400 kms^{-1} given in Cho et al. (2007) at $\sim 1.6 - 2.1\,\mathrm{R}_\odot$. The Alfvén speed of the order of 140 kms^{-1} to 460 kms^{-1} at heliocentric distance $\sim 1.2 - 1.5\,\mathrm{R}_\odot$ reported in Gopalswamy et al. (2011a), while Kim et al. (2012) inferred Alfvén speed in the range of 259 - 982 kms^{-1} over 3 - 15 $\mathrm{R}_\odot$. The shock speed estimated agrees well with the works of Cunha-Silva et al. (2015) and Minta et al. (2023) who found shock speed of the order of 200 kms^{-1} to 810 kms^{-1}. Using Rankine-Hugoniot approximation, the Mach number of the order of 1.1 to 1.8 is obtained and the magnetic field strength in the range of $\sim 7.8 - 0.7\,G$ which is fitted with a single power-law s $B(r) = 6.1r^{-3.89}\,G$ at the same heliocentric distance. The range of Mach number is in good agreement with the range of Mach number of $1.59 < \mathrm{M_A} < 2.53$ reported by Mann et al. (2022) and $\mathrm{M_A} \geq 1.5$ by Su et al. (2022). Our magnetic field strength estimate of the order $\sim 7.8 - 0.7\,G$ at $\sim 1 - 2\,\mathrm{R}_\odot$ is well consistent with the work of Vršnak et al. (2002) who reported the magnetic field strength of 1 - 8 G at $\sim 1.6\,\mathrm{R}\odot$ and also with 6 - 5 G at $\sim 1.5 - 1.7\,\mathrm{R}\odot$ found in Ramesh et al. (2010). According to the current research, 18 of the 31 type II radio events are

precursors for space weather because they are connected to immediate space weather phenomena like radio blackouts and polar cap absorption events, exhibit band-splitting characteristics, or are followed by type III and IV bursts. The results from current study also indicate that analyzed SRBs were associate by ionospheric disturbances as demonstrated by TEC enhancement. The findings of this study demonstrate that it is possible to track well the progress of solar cycle 25 and forecast the intensity of associated space weather phenomena by analyzing and characterizing the physical features accompanying Type II SRBs observed from the ground (Ndacyayisenga et al., 2021a).

Author contributions. T. Ndacyayisenga, Jean Uwamahoro and D. Okoh conceived the presented idea and the design of the study. T. Ndacyayisenga manually gathered the data used. C. Monstein and D. Okoh, helped in programming for data analysis. Analysis and intrepretation of the results are done by T Ndacyayisenga who later drafted the manuscript. This manuscript is reviewed by Jean Uwamahoro, J. C Uwamahoro, Rabiu Babatunde, D. Okoh, K. Sasikumar Raja and C. Kwisanga.

Competing interests. The authors declare that the research was conducted in the absence of any commercial or financial relationships that could be created as a potential conflict of interest.

Acknowledgements. This work was supported by International Science Programme (ISP) through Rwanda Astrophysics, Space and Climate Science Research Group (RASCSRG) and Centre for atmospheric Research through National Space Research and Development Agency, Abuja, Nigeria. We thank FHNW, Institute for Data Science in Brugg/Windisch, Switzerland for hosting the e-Callisto network. The authors also thank the providers of all the data used from SOHO/LASCO; NOAA; GOES, SWPC, African Geodetic Reference Frame (http://afrefdata.org), WDC-SILSO and the UNAVCO Archive of GNSS Data (ftp://data-out.unavco.org). The author (C. Monstein) thanks the ISSI - Bern International Team of 'Why Ionospheric Dynamics and Structure Behave Differently in The African Sector' (the team leaders E. Yizengaw & K. Groves) for valuable discussions about part of the results that are included in this paper.

References

Ahluwalia, H. S.: Forecast for sunspot cycle 25 activity, Advances in Space Research, 69, 794–797, https://doi.org/10.1016/j.asr.2021.09.035, 2022.

Amory-Mazaudier, C., Menvielle, M., Curto, J.-J., and Le Huy, M.: Recent Advances in Atmospheric, Solar-Terrestrial Physics and Space Weather From a North-South network of scientists [2006-2016] PART A: TUTORIAL, Sun and Geosphere, 12, 1–19, 2017.

Benz, A. O., Monstein, C., and Meyer, H.: Callisto A New Concept for Solar Radio Spectrometers, Sol. Phys., 226, 143–151, https://doi.org/10.1007/s11207-005-5688-9, 2005.

Benz, A. O., Monstein, C., Meyer, H., Manoharan, P. K., Ramesh, R., Altyntsev, A., Lara, A., Paez, J., and Cho, K. S.: A World-Wide Net of Solar Radio Spectrometers: e-CALLISTO, Earth Moon and Planets, 104, 277–285, https://doi.org/10.1007/s11038-008-9267-6, 2009.

Brajša, R., Verbanac, G., Bandić, M., Hanslmeier, A., Skokić, I., and Sudar, D.: A prediction for the 25th solar cycle maximum amplitude, Astronomische Nachrichten, 343, e13960, https://doi.org/10.1002/asna.202113960, 2022.

Brueckner, G. E., Howard, R. A., Koomen, M. J., Korendyke, C. M., Michels, D. J., Moses, J. D., Socker, D. G., Dere, K. P., Lamy, P. L., Llebaria, A., Bout, M. V., Schwenn, R., Simnett, G. M., Bedford, D. K., and Eyles, C. J.: The Large Angle Spectroscopic Coronagraph (LASCO), Sol. Phys., 162, 357–402, https://doi.org/10.1007/BF00733434, 1995.

Cairns, I. H., Knock, S. A., Robinson, P. A., and Kuncic, Z.: Type II Solar Radio Bursts: Theory and Space Weather Implications, Space Sci. Rev., 107, 27–34, https://doi.org/10.1023/A:1025503201687, 2003.

Cane, H. V. and Erickson, W. C.: Studies of Space Weather Using Solar Radio Bursts, in: From Clark Lake to the Long Wavelength Array: Bill Erickson's Radio Science, edited by Kassim, N., Perez, M., Junor, W., and Henning, P., vol. 345 of *Astronomical Society of the Pacific Conference Series*, p. 133, 2005.

Carley, E. P., Vilmer, N., Simões, P. J. A., and Ó Fearraigh, B.: Estimation of a coronal mass ejection magnetic field strength using radio observations of gyrosynchrotron radiation, A&A, 608, A137, https://doi.org/10.1051/0004-6361/201731368, 2017.

Chernov, G. and Fomichev, V.: On the Issue of the Origin of Type II Solar Radio Bursts, ApJ, 922, 82, https://doi.org/10.3847/1538-4357/ac1f32, 2021.

Cho, K. S., Lee, J., Gary, D. E., Moon, Y. J., and Park, Y. D.: Magnetic Field Strength in the Solar Corona from Type II Band Splitting, ApJ, 665, 799–804, https://doi.org/10.1086/519160, 2007.

Cho, K.-S., Gopalswamy, N., Kwon, R.-Y., Kim, R.-S., and Yashiro, S.: A HIGH-FREQUENCY TYPE II SOLAR RADIO BURST ASSOCIATED WITH THE 2011 FEBRUARY 13 CORONAL MASS EJECTION, The Astrophysical Journal, 765, 148, https://doi.org/10.1088/0004-637X/765/2/148, 2013.

Cunha-Silva, R. D., Fernandes, F. C. R., and Selhorst, C. L.: Solar type II radio bursts associated with CME expansions as shown by EUV waves, A& A, 578, A38, https://doi.org/10.1051/0004-6361/201425388, 2015.

Du, Z. L.: The solar cycle: predicting the peak of solar cycle 25, Astrophysics and Space Science, 365, 104, https://doi.org/10.1007/s10509-020-03818-1, 2020.

Dulk, G. A. and McLean, D. J.: Coronal magnetic fields., Sol. Phys., 57, 279–295, https://doi.org/10.1007/BF00160102, 1978.

Fleishman, G. D., Gary, D. E., Chen, B., Kuroda, N., Yu, S., and Nita, G. M.: Decay of the coronal magnetic field can release sufficient energy to power a solar flare, Science, 367, 278–280, https://doi.org/10.1126/science.aax6874, 2020.

Gopalswamy, N.: Coronal Mass Ejections and Solar Radio Emissions, in: Planetary, Solar and Heliospheric Radio Emissions (PRE VII), edited by Rucker, H. O., Kurth, W. S., Louarn, P., and Fischer, G., pp. 325–342, 2011.

Gopalswamy, N. and Yashiro, S.: THE STRENGTH AND RADIAL PROFILE OF THE CORONAL MAGNETIC FIELD FROM THE STANDOFF DISTANCE OF A CORONAL MASS EJECTION-DRIVEN SHOCK, The Astrophysical Journal Letters, 736, L17, https://doi.org/10.1088/2041-8205/736/1/L17, 2011.

Gopalswamy, N., Lara, A., Kaiser, M. L., and Bougeret, J. L.: Near-Sun and near-Earth manifestations of solar eruptions, J. Geophys. Res., 106, 25 261–25 278, https://doi.org/10.1029/2000JA004025, 2001.

Gopalswamy, N., Nitta, N., Akiyama, S., Mäkelä, P., and Yashiro, S.: CORONAL MAGNETIC FIELD MEASUREMENT FROM EUV IMAGES MADE BY THE SOLAR DYNAMICS OBSERVATORY, The Astrophysical Journal, 744, 72, https://doi.org/10.1088/0004-637x/744/1/72, 2011a.

Gopalswamy, N., Nitta, N., Akiyama, S., Mäkelä, P., and Yashiro, S.: CORONAL MAGNETIC FIELD MEASUREMENT FROM EUV IMAGES MADE BY THE SOLAR DYNAMICS OBSERVATORY, The Astrophysical Journal, 744, 72, https://doi.org/10.1088/0004-637X/744/1/72, 2011b.

Gopalswamy, N., Xie, H., Mäkelä, P., Yashiro, S., Akiyama, S., Uddin, W., Srivastava, A., Joshi, N., Chandra, R., Manoharan, P., Mahalakshmi, K., Dwivedi, V., Jain, R., Awasthi, A., Nitta, N., Aschwanden, M., and Choudhary, D.: Height of shock formation in the solar corona inferred from observations of type II radio bursts and coronal mass ejections, Advances in Space Research, 51, 1981–1989, https://doi.org/https://doi.org/10.1016/j.asr.2013.01.006, 2013.

Gopalswamy, N., Yashiro, S., Mäkelä, P., Xie, H., Akiyama, S., and Monstein, C.: Extreme Kinematics of the 2017 September 10 Solar Eruption and the Spectral Characteristics of the Associated Energetic Particles, The Astrophysical Journal, 863, L39, https://doi.org/10.3847/2041-8213/aad86c, 2018.

Grechnev, V. V., Afanasyev, A. N., Uralov, A. M., Chertok, I. M., Eselevich, M. V., Eselevich, V. G., Rudenko, G. V., and Kubo, Y.: Coronal Shock Waves, EUV Waves, and Their Relation to CMEs. III. Shock-Associated CME/EUV Wave in an Event with a Two-Component EUV Transient, Sol. Phys., 273, 461–477, https://doi.org/10.1007/s11207-011-9781-y, 2011.

Kallunki, J., McKay, D., and Tornikoski, M.: First Type III Solar Radio Bursts of Solar Cycle 25, Sol. Phys., 296, 57, https://doi.org/10.1007/s11207-021-01790-9, 2021.

Kavanagh, A., Marple, S., Honary, F., McCrea, I., and Senior, A.: On solar protons and polar cap absorption: constraints on an empirical relationship, Annales Geophysicae, 22, 1133–1147, https://doi.org/10.5194/angeo-22-1133-2004, 2004.

Kim, R.-S., Gopalswamy, N., Moon, Y.-J., Cho, K.-S., and Yashiro, S.: MAGNETIC FIELD STRENGTH IN THE UPPER SOLAR CORONA USING WHITE-LIGHT SHOCK STRUCTURES SURROUNDING CORONAL MASS EJECTIONS, The Astrophysical Journal, 746, 118, https://doi.org/10.1088/0004-637x/746/2/118, 2012.

Kishore, P., Ramesh, R., Hariharan, K., Kathiravan, C., and Gopalswamy, N.: CONSTRAINING THE SOLAR CORONAL MAGNETIC FIELD STRENGTH USING SPLIT-BAND TYPE II RADIO BURST OBSERVATIONS, 832, 59, https://doi.org/10.3847/0004-637X/832/1/59, 2016.

Kouloumvakos, A., Rouillard, A., Warmuth, A., Magdalenic, J., Jebaraj, I. C., Mann, G., Vainio, R., and Monstein, C.: Coronal Conditions for the Occurrence of Type II Radio Bursts, ApJ, 913, 99, https://doi.org/10.3847/1538-4357/abf435, 2021.

Kumari, A., Ramesh, R., Kathiravan, C., and Wang, T. J.: Addendum to: Strength of the Solar Coronal Magnetic Field - A Comparison of Independent Estimates Using Contemporaneous Radio and White-Light Observations, Sol. Phys., 292, 177, https://doi.org/10.1007/s11207-017-1203-3, 2017.

350   Kumari, A., Ramesh, R., Kathiravan, C., Wang, T. J., and Gopalswamy, N.: Direct Estimates of the Solar Coronal Magnetic Field Using Contemporaneous Extreme-ultraviolet, Radio, and White-light Observations, The Astrophysical Journal, 881, 24, https://doi.org/10.3847/1538-4357/ab2adf, 2019.

Kumari, A., Morosan, D. E., and Kilpua, E. K. J.: On the Occurrence of Type IV Solar Radio Bursts in Solar Cycle 24 and Their Association with Coronal Mass Ejections, ApJ, 906, 79, https://doi.org/10.3847/1538-4357/abc878, 2021.

355   Lata Soni, S., Ebenezer, E., and lal Yadav, M.: Multi-wavelength analysis of CME-driven shock and Type II solar radio burst band-splitting, Astrophys Space Sci, 366, 31, https://doi.org/10.1007/s10509-021-03933-7, 2021.

Leblanc, Y., Dulk, G. A., and Bougeret, J.-L.: Tracing the Electron Density from the Corona to 1au, Sol. Phys., 183, 165–180, https://doi.org/10.1023/A:1005049730506, 1998.

Maguire, C. A., Carley, E. P., McCauley, J., and Gallagher, P. T.: Evolution of the Alfvén Mach number associated with a coronal mass
360   ejection shock, A & A, 633, A56, https://doi.org/10.1051/0004-6361/201936449, 2020.

Maia, D., Pick, M., Vourlidas, A., and Howard, R.: Development of Coronal Mass Ejections: Radio Shock Signatures, The Astrophysical Journal, 528, L49–L51, https://doi.org/10.1086/312421, 2000.

Mann, G., Vocks, C., Warmuth, A., Magdalenic, J., Bisi, M., Carley, E., Dabrowski, B., Gallagher, P., Krankowski, A., Maty-jasiak, B., Rotkaehl, H., and Zucca, P.: Excitation of Langmuir waves at shocks and solar type II radio bursts, A&A, 660, A71,
365   https://doi.org/10.1051/0004-6361/202142201, 2022.

Minta, F. N., Nozawa, S., Kamen, K., Elsaid, A., and Ayman, A.: Assessing the spectral characteristics of band splitting type II radio bursts observed by CALLISTO spectrometers, arXiv e-prints, arXiv:2301.13839, https://doi.org/10.48550/arXiv.2301.13839, 2023.

Mitra, A. P.: Polar Cap Absorption Events, pp. 252–278, Springer Netherlands, Dordrecht, https://doi.org/10.1007/978-94-010-2231-6_11, 1974.

370   Ndacyayisenga, T., Umuhire, A. C., Uwamahoro, J., and Monstein, C.: Space weather study through analysis of solar radio bursts detected by a single-station CALLISTO spectrometer, Annales Geophysicae, 39, 945–959, https://doi.org/10.5194/angeo-39-945-2021, 2021a.

Ndacyayisenga, T., Uwamahoro, J., Sasikumar Raja, K., and Monstein, C.: A statistical study of solar radio Type III bursts and space weather implication, Advances in Space Research, 67, 1425–1435, https://doi.org/https://doi.org/10.1016/j.asr.2020.11.022, 2021b.

Nedal, M., Mahrous, A., and Youssef, M.: Predicting the arrival time of CME associated with type-II radio burst using neural networks
375   technique, Ap & Space Sci., 364, 161, https://doi.org/10.1007/s10509-019-3651-8, 2019.

Newkirk, Gordon, J.: Structure of the Solar Corona, Annu. Rev. Astron. Astrophys., 5, 213, https://doi.org/10.1146/annurev.aa.05.090167.001241, 1967.

Nindos, A.: Incoherent Solar Radio Emission, Frontiers in Astronomy and Space Sciences, 7, 57, https://doi.org/10.3389/fspas.2020.00057, 2020.

380   Nindos, A., Aurass, H., Klein, K. L., and Trottet, G.: Radio Emission of Flares and Coronal Mass Ejections. Invited Review, Sol. Phys., 253, 3–41, https://doi.org/10.1007/s11207-008-9258-9, 2008.

Payne-Scott, R., Yabsley, D. E., and Bolton, J. G.: Relative Times of Arrival of Bursts of Solar Noise on Different Radio Frequencies, Nature, 160, 256–257, https://doi.org/10.1038/160256b0, 1947.

Perrone, L., Alfonsi, L., Romano, V., and Franceschi, G.: Polar cap absorption events of November 2001 at Terra Nova Bay, Antarctica,
385   Annales Geophysicae, 22, 1633–1648, https://doi.org/10.5194/angeo-22-1633-2004, 2004.

Pick, M., Forbes, T. G., Mann, G., Cane, H. V., Chen, J., Ciaravella, A., Cremades, H., Howard, R. A., Hudson, H. S., Klassen, A., Klein, K. L., Lee, M. A., Linker, J. A., Maia, D., Mikic, Z., Raymond, J. C., Reiner, M. J., Simnett, G. M., Srivastava, N., Tripathi, D., Vainio,

R., Vourlidas, A., Zhang, J., Zurbuchen, T. H., Sheeley, N. R., and Marqué, C.: Multi-Wavelength Observations of CMEs and Associated Phenomena. Report of Working Group F, Space Sci. Rev., 123, 341–382, https://doi.org/10.1007/s11214-006-9021-1, 2006.

390 Ramesh, R., Kathiravan, C., and Sastry, C. V.: ESTIMATION OF MAGNETIC FIELD IN THE SOLAR CORONAL STREAMERS THROUGH LOW FREQUENCY RADIO OBSERVATIONS, The Astrophysical Journal, 711, 1029–1032, https://doi.org/10.1088/0004-637x/711/2/1029, 2010.

Ranta, H., Ranta, A., Yousef, S. M., Burns, J., and Stauning, P.: D-region observations of polar cap absorption events during the EISCAT operation in 1981-1989., Journal of Atmospheric and Terrestrial Physics, 55, 751–766, https://doi.org/10.1016/0021-9169(93)90018-T, 395 1993.

Reid, H. A. S. and Ratcliffe, H.: A review of solar type III radio bursts, Research in Astronomy and Astrophysics, 14, 773–804, https://doi.org/10.1088/1674-4527/14/7/003, 2014.

Saito, K., Poland, A. I., and Munro, R. H.: A study of the background corona near solar minimum., Sol. Phys., 55, 121–134, https://doi.org/10.1007/BF00150879, 1977.

400 Salmane, H., Weber, R., Abed-Meraim, K., Klein, K.-L., and Bonnin, X.: A method for the automated detection of solar radio bursts in dynamic spectra, Journal of Space Weather and Space Climate, 8, A43, https://doi.org/10.1051/swsc/2018028, 2018.

Sarp, V., Kilcik, A., Yurchyshyn, V., Rozelot, J. P., and Ozguc, A.: Prediction of solar cycle 25: a non-linear approach, MNRAS, 481, 2981–2985, https://doi.org/10.1093/mnras/sty2470, 2018.

Sasikumar Raja, K., Ramesh, R., Hariharan, K., Kathiravan, C., and Wang, T. J.: An Estimate of the Magnetic Field Strength Associated 405 with a Solar Coronal Mass Ejection from Low Frequency Radio Observations, ApJ, 796, 56, https://doi.org/10.1088/0004-637X/796/1/56, 2014.

Sasikumar Raja, K., Venkata, S., Singh, J., and Raghavendra Prasad, B.: Solar coronal magnetic fields and sensitivity requirements for spectropolarimetry channel of VELC onboard Aditya-L1, Advances in Space Research, 69, 814–822, https://doi.org/10.1016/j.asr.2021.10.053, 2022.

410 Seemala, G. K. and Valladares, C. E.: Statistics of total electron content depletions observed over the South American continent for the year 2008, Radio Science, 46, https://doi.org/https://doi.org/10.1029/2011RS004722, 2011.

Shea, M. A. and Smart, D. F.: Solar proton event patterns: the rising portion of five solar cycles, Advances in Space Research, 29, 325–330, https://doi.org/10.1016/S0273-1177(01)00592-0, 2002.

Smerd, S. F., Sheridan, K. V., and Stewart, R. T.: On Split-Band Structure in Type II Radio Bursts from the Sun (presented by S.F. Smerd), 415 in: Coronal Disturbances, edited by Newkirk, G. A., vol. 57, p. 389, 1974.

Smerd, S. F., Sheridan, K. V., and Stewart, R. T.: Split-Band Structure in Type II Radio Bursts from the Sun, Astrophys. Lett., 16, 23, 1975.

Smith, A. R. A., Beggan, C. D., Macmillan, S., and Whaler, K. A.: Climatology of the Auroral Electrojets Derived From the Along-Track Gradient of Magnetic Field Intensity Measured by POGO, Magsat, CHAMP, and Swarm, Space Weather, 15, 1257–1269, https://doi.org/10.1002/2017SW001675, 2017.

420 Su, W., Li, T. M., Cheng, X., Feng, L., Zhang, P. J., Chen, P. F., Ding, M. D., Chen, L. J., Guo, Y., Wang, Y., Li, D., and Zhang, L. Y.: Quantifying the Magnetic Structure of a Coronal Shock Producing a Type II Radio Burst, The Astrophysical Journal, 929, 175, https://doi.org/10.3847/1538-4357/ac5fac, 2022.

SW: SOLAR CYCLE UPDATE. Retrieved from https://spaceweather.com/archive.php?view=1&day=12&month=01&year=2022, Accessed on 18 July 2022, p. 1, 2022.

Tan, B.: Multi-timescale solar cycles and the possible implications, Astrophysics and Space Science, 332, 65–72, https://doi.org/10.1007/s10509-010-0496-6, 2011.

Tan, B., Chen, N., Yang, Y.-H., Tan, C., Masuda, S., Chen, X., and Misawa, H.: Solar Fast-drifting Radio Bursts in an X1.3 Flare on 2014 April 25, The Astrophysical Journal, 885, 90, https://doi.org/10.3847/1538-4357/ab4718, 2019.

Temmer, M., Veronig, A. M., Kontar, E. P., Krucker, S., and Vršnak, B.: Combined STEREO/RHESSI Study of Coronal Mass Ejections Acceleration and Particle Acceleration in Solar Flares, The Astrophysical Journal, 712, 1410–1420, https://doi.org/10.1088/0004-637x/712/2/1410, 2010.

Umuhire, A. C., Gopalswamy, N., Uwamahoro, J., Akiyama, S., Yashiro, S., and Mäkelä, P.: Properties of High-Frequency Type II Radio Bursts and Their Relation to the Associated Coronal Mass Ejections, Sol. Phys., 296, 27, https://doi.org/10.1007/s11207-020-01743-8, 2021.

Uwamahoro, J. C., Giday, N. M., Habarulema, J. B., Katamzi-Joseph, Z. T., and Seemala, G. K.: Reconstruction of Storm-Time Total Electron Content Using Ionospheric Tomography and Artificial Neural Networks: A Comparative Study Over the African Region, Radio Science, 53, 1328–1345, https://doi.org/10.1029/2017RS006499, 2018.

Vasanth, V., Umapathy, S., Vršnak, B., and Anna Lakshmi, M.: Characteristics of Type-II Radio Bursts Associated with Flares and CMEs, Sol. Phys., 273, 143–162, https://doi.org/10.1007/s11207-011-9854-y, 2011.

Vasanth, V., Umapathy, S., Vršnak, B., Žic, T., and Prakash, O.: Investigation of the Coronal Magnetic Field Using a Type II Solar Radio Burst, Sol. Phys., 289, 251–261, https://doi.org/10.1007/s11207-013-0318-4, 2014.

Vemareddy, P., Démoulin, P., Sasikumar Raja, K., Zhang, J., Gopalswamy, N., and Vasantharaju, N.: Eruption of the EUV Hot Channel from the Solar Limb and Associated Moving Type IV Radio Burst, ApJ, 927, 108, https://doi.org/10.3847/1538-4357/ac4dfe, 2022.

Vourlidas, A., Carley, E. P., and Vilmer, N.: Radio Observations of Coronal Mass Ejections: Space Weather Aspects, Frontiers in Astronomy and Space Sciences, 7, 43, https://doi.org/10.3389/fspas.2020.00043, 2020.

Vršnak, B., Aurass, H., Magdalenić, J., and Gopalswamy, N.: Band-splitting of coronal and interplanetary type II bursts. I. Basic properties, A & A, 377, 321–329, https://doi.org/10.1051/0004-6361:20011067, 2001.

Vršnak, B., Magdalenić, J., Aurass, H., and Mann, G.: Band-splitting of coronal and interplanetary type II bursts. II. Coronal magnetic field and Alfvén velocity, A & A, 396, 673–682, https://doi.org/10.1051/0004-6361:20021413, 2002.

Wild, J. P. and McCready, L. L.: Observations of the Spectrum of High-Intensity Solar Radiation at Metre Wavelengths. I. The Apparatus and Spectral Types of Solar Burst Observed, Australian Journal of Scientific Research A Physical Sciences, 3, 387, https://doi.org/10.1071/CH9500387, 1950.

Wild, J. P., Smerd, S. F., and Weiss, A. A.: Solar Bursts, Ann. Rev. Astron and Astrophys., 1, 291, https://doi.org/10.1146/annurev.aa.01.090163.001451, 1963.

Zucca, P., Morosan, D. E., Rouillard, A. P., Fallows, R., Gallagher, P. T., Magdalenic, J., Klein, K. L., Mann, G., Vocks, C., Carley, E. P., Bisi, M. M., Kontar, E. P., Rothkaehl, H., Dabrowski, B., Krankowski, A., Anderson, J., Asgekar, A., Bell, M. E., Bentum, M. J., Best, P., Blaauw, R., Breitling, F., Broderick, J. W., Brouw, W. N., Brüggen, M., Butcher, H. R., Ciardi, B., de Geus, E., Deller, A., Duscha, S., Eislöffel, J., Garrett, M. A., Grießmeier, J. M., Gunst, A. W., Heald, G., Hoeft, M., Hörandel, J., Iacobelli, M., Juette, E., Karastergiou, A., van Leeuwen, J., McKay-Bukowski, D., Mulder, H., Munk, H., Nelles, A., Orru, E., Paas, H., Pandey, V. N., Pekal, R., Pizzo, R., Polatidis, A. G., Reich, W., Rowlinson, A., Schwarz, D. J., Shulevski, A., Sluman, J., Smirnov, O., Sobey, C., Soida, M., Thoudam, S., Toribio, M. C., Vermeulen, R., van Weeren, R. J., Wucknitz, O., and Zarka, P.: Shock location and CME 3D reconstruction of a solar type II radio burst with LOFAR, A & A, 615, A89, https://doi.org/10.1051/0004-6361/201732308, 2018.